# Bayesian segmentation for damage image using MRF prior

G. Li[1], F.G. Yuan[1], R. Haftka[2] and N. H. Kim[2]
[1]Department of Mechanical and Aerospace Engineering,
North Carolina State University, Raleigh, NC, 27695-7921, USA
[2]Department of Mechanical and Aerospace Engineering,
University of Florida, Gainesville, FL 32611, USA

## ABSTRACT

Image segmentation for quantifying damage based on Bayesian updating scheme is proposed for diagnosis and prognosis in structural health monitoring. This scheme enables taking into account the prior information of the state of the structures, such as spatial constraints and image smoothness. Bayes' law is employed to update the segmentation with the spatial constraint described as Markov Random Field and the current observed image acting as a likelihood function. Segmentation results demonstrate that the proposed algorithm holds promise of searching a crack area in the SHM image and focusing on the real damage area by eliminating the pseudo-shadow area. Thus more precise crack estimation can be obtained than the conventional *K*-means segmentation by shrinking the fuzzy tails which often exist on both sides of the crack tips.

**Keywords:** Damage imaging, Damage estimation, Image segmentation, Markov random field, Gibbs random field.

## 1. INTRODUCTION

Aircraft plate-like structures are prone to develop cracks due to cyclic loads and severely corrosive service environments. Diagnosis and prognosis of damage are essential issues in structural health monitoring for preventing catastrophic failures and predicting the remaining life of structures. Ultrasonic wave imaging with various sensor array forms has potential to detect the damage or abnormity on large-scale, complex plate-like structures. Damage location, shape and severity evaluation is one of the most important topics in structural health monitoring. The Lamb wave imaging method has been recently shown to be effective in detecting damage such as crack or delamination in structures [1][2][3]. Damage imaging methods have focused on time-reversal based migration technique in both time-space domain and frequency-wave number domain [4][5][6][7]. These methods can generate images indicating the damage condition of structures by interpolating the data measured from different forms of sensor arrays.

The paper aims at quantifying the damage based on the images generated from existing imaging techniques. Since the size of the crack provides the essential information for structural health prognosis to estimate residual life of the structural component according to crack propagation law such as Paris law [8] in metals, which relates stress intensity factor and crack growth under fatigue. Image segmentation is an image processing technique, which separates the whole detected image into several meaningful regions with homogeneous attributes, e.g., damaged regions/non-damaged regions, according to the image itself and some prior knowledge. Figure 1 shows a typical intensity image and its segmentation. Although human diagnosis with experience can identify the segmented regions from the observed image, but it is not an easy job for a computer to automatically divide an observed image (especially noise contaminated images with fuzzy information) into meaningful regions. Image segmentation based on statistical models has been developed in medical image analysis [9][10] and computer vision [11] [12] [13]. Bayesian updating scheme used for image segmentation is introduced to merge the observed image data with the prior knowledge, including spatial constraints, strength and distribution of disturbance to achieve more precise segmentation results than those obtained using traditional image segmentation method like *K*-means method [14].

The service environments and specific aircraft structures lead to the following three main properties of the detected images using ultrasonic waves when compared to medical imaging technique for human bodies. First, the large scale of aircraft structures and online diagnostic requirements promote relative low density of sensor distribution. Second, severe variations of temperature and humidity during the in-flight service alter the dynamic response of detected structures. Third, due to noise, electromagnetic disturbances from the environment, the monitoring system itself and structural

Sensors and Smart Structures Technologies for Civil, Mechanical, and Aerospace Systems 2009
edited by Masayoshi Tomizuka, Chung-Bang Yun, Victor Giurgiutiu, Proc. of SPIE Vol. 7292
72920J · © 2009 SPIE · CCC code: 0277-786X/09/$18 · doi: 10.1117/12.816507

vibrations, the experimental images from SHM ultrasonic wave diagnosis are always of relatively low quality. It is difficult for the traditional image segmentation like the threshold method, *K*-means clustering to effectively separate the damage region from the background. A reliable image segmentation scheme, which can be relatively immune to noise and fuzzy tails, is imperative to obtain a meaningful segmentation and precise damage quantification.

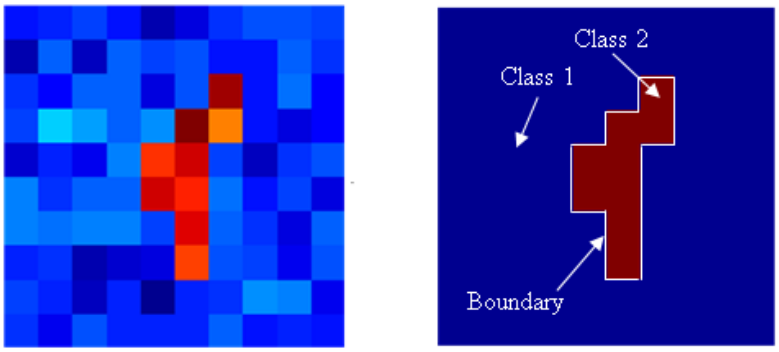


Figure 1 An Image of intensity and its binary segmentation

In this paper, image segmentation based on Bayesian updating with Markov Random Field is investigated for plate-like structural health monitoring using ultrasonic guided Lamb waves. This paper is organized as follows. Section 2 introduces the Bayesian updating concept in image segmentation. Section 3 introduces Markov Random Field and Gibbs Random Field as prior information in the Bayesian updating framework. Section 4 discusses how to model the image segmentation problem with Bayesian updating framework, and to quantify the image segmentation as a problem of maximizing a posterior (MAP). An illustrative example is also given in this section. Section 5 presents the application of the segmentation method for reverse-time migration image in frequency-wavenumber domain. Section 6 carries out some discussion on the results. Section 7 provides concluding remarks.

## 2. IMAGE SEGMENTATION BASED ON BAYESIAN UPDATING

Image segmentation refers to the process of partitioning an image into multiple regions. The goal of segmentation is to simplify the representation of an image into a class of certain representations, each of which holds distinct characteristic and is easier to distinguish among them. Researchers have developed many methods based on traditional clustering method such as fuzzy mathematics, neural network, and statistical models. Bayesian updating is one viable approach, which takes advantage of a statistical model to combine the current observed data with prior knowledge, such as spatial constraints and smoothness level.

Bayesian updating is statistical inference in which evidence or observations are used to update or to newly infer the probability that a hypothesis may be true. It uses aspects of the scientific method, which involves collecting evidence that is meant to be consistent or inconsistent with a given hypothesis. As evidence accumulates, the degree of belief in a hypothesis should change. With enough evidence, it should become very high or very low.

Thomas Bayes firstly introduced Bayesian theorem [15], which relates the conditional and marginal probabilities of events $x$ and $y$ by

$$p(x \mid y) = \frac{p(y \mid x)p(x)}{p(y)} \tag{1}$$

Where,

$p(x)$ is the prior probability or marginal probability of $x$ before the observation. It is 'prior' in the sense that it does not take into account any information about $y$.

$p(x \mid y)$ is the conditional probability of $x$ after the observation, given $y$. It is also called the posterior probability because it is derived from or depends upon the specified value of $y$.

$p(y \mid x)$ is the likelihood function, which is the conditional probability of $y$ given $x$.

$p(y)$ is marginal probability of $y$, and acts as a normalizing constant.

In image segmentation, the prior function $p(x)$ can represent prior assumptions about the image for monitoring the structural health. For instance, the assumption can include how the pixels constrain each other in the space, and how severe the environmental noise is. In addition, a previous monitoring image and prior knowledge about the structure can also be considered as prior information. The likelihood function relates to the observed information, which is the detected intensity image in diagnosis from guided wave imaging with finite sensor array, such as linear sensor array [16] or distributed sensor array [17].

## 3. MARKOV RANDOM FIELD AND GIBBS RANDOM FIELD

Markov Random Field (MRF) image modeling has been used successfully in many image processing techniques [18]. The success of Markov Random Field modeling mainly arises from its systematic and flexible treatment of the contextual information in the image. Prior knowledge about the image segmentation can be easily quantified by Markov Random Field model parameters. Image segmentation processes the property of contextual smoothness of the class labels in the image space so that a pixel with a particular class label is likely to share the label with its immediate neighbors. Moreover a Bayesian framework using MRF provides feasible optimal solutions. The optimization process using spatial local interaction makes parallel and local computations possible. Following are some basic definitions [19] and derivations for the image segmentation based on Bayesian updating scheme.

Neighborhood

A neighborhood system $\eta$ associated with the whole image $\Omega$ is a collection of neighborhoods $\eta = \{\eta_s \mid s \in \Omega\}$, where each $\eta_s$ is a neighborhood of the pixel at the site of $s$ satisfying

(1) The pixel itself does not belong to its own neighborhood, or $s \notin \eta_s$;

(2) The pixel $s$ belonging to the neighborhood of pixel $t$ implies that pixel $t$ belongs to the neighborhood of pixel $s$, or $s \in \eta_t$ implies $t \in \eta_s$

Clique

A clique is a subset $C$ of the whole image $\Omega$ if two different element of $C$ are neighbors. Figure 2 gives the 2nd order neighborhood and all the available cliques in this 8-element neighboring system.

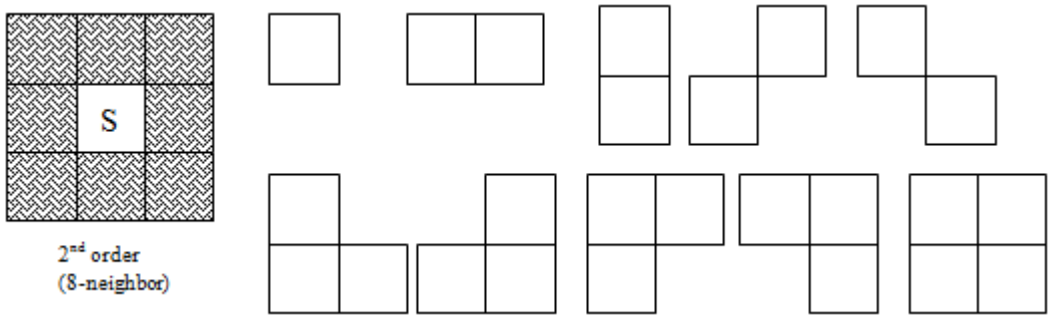


Figure 2 All possible cliques for the second-order neighborhood system

Markov Random Field

A Markov Random Field on $(\Omega, \eta)$ is a random field with its probability property of each site in the whole field satisfying the Markovian property described as following,

$P(X_s = x_s \mid X_t = x_t, \forall t \in \Omega, t \neq s) = P(X_s = x_s \mid X_t = x_t, t \in \eta_s), \forall \in \Omega$ .

Gibbs Random Field

A random field $X$ with ($\Omega$, $\eta$, $C$), is a Gibbs Random Field (GRF, or a random field with a Gibbs distribution) if its joint distribution has the form

$$P(x) = \frac{1}{Z}\exp\left(\sum_{c \in C} V_c(x)\right) \tag{2}$$

where $C$ is the set of all cliques in $\Omega$, $Z$ is the normalizing constant, and $V_c(x)$ is the clique potential associated with clique $c$. There is no particular restriction on the clique potential definition. As long as the resulting Gibbs distribution satisfies the definition of the probability, the associated clique potentials are valid. The Gibbs potential can be defined such that some specific features of the image can be identified and emphasized. In addition, it is not necessary to use all types of cliques for a given neighborhood system; that is, any specific set of clique types can be selectively used.

A Gibbs Random Field is defined by a joint probability. On the contrary, the MRF is defined based on a conditional probability. Prior Knowledge about the problem such as the smoothness constraint on the class label can be incorporated into the Gibbs distribution by the choice of specific clique types and their potentials. For example, the smoothness of the class label in image space can be measured by defining the clique potential such that a high positive clique potential is assigned only when all class label in the clique are identical.

Hammersley-Clifford Theorem

On ($\Omega$, $\eta$, $C$), a random field $X$ is a Markov random field with respect to $\eta$ if and only if $P(x)$ has a Gibbs distribution with respect to $\eta$. Hammersley-Clifford Theorem builds a bridge between MRF and GRF. The joint distribution (i.e., Gibbs distribution) can be constructed from the local conditional probability (i.e. MRF). As a sequence of the theorem, it is now possible to express the conditional probability of a Markov Random Field in terms of clique potentials. This is useful in practice because it is easy choose the clique types and their potentials to describe the desired local behavior. For example, local spatial relationships such as smoothness and continuity of the neighboring pixels can be specified by isotropic pair clique potential $\beta$. It is crucial for the theorem to share the same neighborhood system $\eta$ and the associate clique $c$ for both MRF and GRF.

## 4. PROBLEM MODELING WITH MAXIMUM A POSTERIOR

### 4.1 Bayesian updating with MRF/GRF

The image constructed by the signals from the sensor array for structural health diagnosis is usually noisy and with fuzzy tails as discussed in Section 1. In Bayesian updating scheme, the current image, which can be considered as a likelihood function, is updated by introducing prior assumption. MRF/GRF discussed in Section 3 is employed to eliminate the effect of noise in the images by designating these similar neighbors with high probability. Thus the segmentation procedure depends on not only the image intensity but also the space restriction property of the neighboring system.

For computational efficiency, the 2nd-order clique is used, which contains an 8-element neighborhood. According to the MRF-GRF equivalence described by Hammersley-Clifford theorem, the clique potential is given in the form of Gibbs density as Eq.(2) The Gibbs potential value is defined as [12],

$$V_C(x) = \begin{cases} -\beta & \text{if } x_s = x_q \text{ and } s, q \in C \\ +\beta & \text{if } x_s \neq x_q \text{ and } s, q \in C \end{cases} \tag{3}$$

where $\beta$ is positive. The choice of $\beta$ will affect the spatial constraint in the GRF. Larger $\beta$ results in stronger spatial constraint; that is, neighbors are more likely to have the same label.

The image segmentation problem is ill-posed simply because its solution space is too large. The solution space can be reduced by incorporating prior knowledge about the image, such as the smoothness in the problem formulation. The *Maximum a posteriori* (MAP) criterion [20] has frequently been used to characterize the prior knowledge. According to the MAP criterion, given a realization of a random field, the goal is to find an optimal realization of $\hat{x}$, which maximizes the a posteriori probability $P(x \mid y)$ for all possible realizations of $x$. By exploiting the chain rule and taking the monotonically increasing logarithmic function, the maximization can be equivalently expressed as:

$$\begin{aligned} \hat{x} &= \arg\max_x P(x \mid y) \\ &= \arg\max_x \frac{P(y \mid x)P(x)}{P(y)} \\ &= \arg\max_x P(y \mid x)P(x) \\ &= \arg\max_x [\ln P(y \mid x) + \ln P(x)] \end{aligned} \tag{4}$$

The observed image can be modeled with a Gaussian distribution [12], and the prior function is the Gibbs Random Field, which holds the probability in Eq. (5). Thus the MAP problem can be described as:

$$p(x \mid y) \propto \exp\left\{-\frac{1}{2\sigma^2}\left[y_s - \mu_s^{x_s}\right]^2 - \sum_C V_C(x)\right\} \tag{5}$$

In this equation, $x$ is the segmentation label ranging from 1 to $k$. $S$ is the position of the estimated grid. $y_s$ is the observed value (obtained image from SHM system). And $\mu_s^{x_s}$ is the mean value in the window with a certain size centered at position $s$. $p(x \mid y)$ is the probability of the evaluated grid belonging to the cluster label $x$, given the intensity of some grid. For the posterior probability, if $p(x=0 \mid y) > p(x=1 \mid y)$, then the estimated $x$ should be 0; and if $p(x=0 \mid y) < p(x=1 \mid y)$, then the estimated $x$ should be 1; thus the estimation of the segmentation label $\hat{x}$ is achieved.

This posterior probability comprises of two parts. The first part is Gaussian distribution likelihood, and the second part is the prior density function -- Gibbs potential. The first part is essentially *K-means* method, which calculates the distance between the evaluated value and the clustering center. For the first likelihood part, if the evaluated pixel value is close to the cluster center, the posterior energy function will be enhanced. The second part is the adjustable part according to the neighboring environment. For the prior– Gibbs potential part, if the neighbor clique member is the same label (from initialization or the previous segmentation), the *Vc(x)* should be negative, then the posterior energy density will be enhanced. On the other hand, if the clique members are at different labels, the posterior energy density will be weakened. For a given case, neglecting the prior distribution by setting $\beta = 0$, this algorithm degenerates to a *K*-means clustering method, which only counts the distance between each point with the clustering centers.

### 4.2 An illustrative example

To illustrate the procedure and the power of the Bayesian based algorithm for SHM image segmentation, a small size grey-level matrix, which represents a simple image of intensity scaling from 0 to 1, is shown in Figure 3.

| | A | B | C | D | E | F | G | H | I | J |
|---|---|---|---|---|---|---|---|---|---|---|
| 1 | 0 | 0 | 0 | 0 | 0 | 0 | 0 | 0 | 0 | 0 |
| 2 | 0 | 0 | 0 | 0 | 0 | 0 | 0 | 0 | 0 | 0 |
| 3 | 0 | 0 | 0 | 0 | 0 | 0 | 0 | 0.77 | 0 | 0 |
| 4 | 0 | 0 | 0 | 0 | 0 | 0 | 0 | 0 | 0 | 0 |
| 5 | 0 | 0 | 0 | 0 | 0 | 0 | 0 | 0 | 0 | 0 |
| 6 | 0 | 0 | 0.9 | 0.7 | 0.75 | 0 | 0 | 0 | 0 | 0 |
| 7 | 0 | 0 | 0.8 | 0.85 | 0 | 0 | 0 | 0 | 0 | 0 |
| 8 | 0 | 0 | 0 | 0 | 0 | 0 | 0 | 0 | 0.8 | 0 |
| 9 | 0 | 0 | 0 | 0 | 0 | 0 | 0 | 0 | 0 | 0 |
| 10 | 0 | 0 | 0 | 0 | 0 | 0 | 0 | 0 | 0 | 0 |

Figure 3 Matrix representation of original image for illustrative example

The image has three patches of high-level areas at the first glance marked as the darker color. The left-side area consisting of elements (0.9, 0.7, 0.75, 0.8 and 0.85) is a relative large area, and the two right-side ones, which are elements 0.77 and 0.8, are small. In image analysis, these small areas are usually caused by environment noise, thus they should be eliminated from the image in the segmentation procedure. Figure 4 is the corresponding noise contaminated matrix, whose intensity image representation can be seen in Figure 3(a).

| | A | B | C | D | E | F | G | H | I | J |
|---|---|---|---|---|---|---|---|---|---|---|
| 14 | 0.04 | 0.02 | 0.03 | 0.04 | 0.16 | 0.10 | 0.00 | 0.06 | 0.06 | 0.04 |
| 15 | 0.17 | 0.07 | 0.13 | 0.07 | 0.03 | 0.06 | 0.03 | 0.03 | 0.08 | 0.01 |
| 16 | 0.01 | 0.06 | 0.07 | 0.08 | 0.11 | 0.05 | 0.11 | 0.73 | 0.09 | 0.06 |
| 17 | 0.03 | 0.22 | 0.16 | 0.07 | 0.14 | 0.17 | 0.19 | 0.03 | 0.10 | 0.06 |
| 18 | 0.11 | 0.01 | 0.07 | 0.13 | 0.08 | 0.06 | 0.04 | 0.15 | 0.02 | 0.04 |
| 19 | 0.12 | 0.01 | 0.99 | 0.77 | 0.80 | 0.06 | 0.09 | 0.02 | 0.02 | 0.09 |
| 20 | 0.12 | 0.11 | 0.93 | 0.97 | 0.02 | 0.04 | 0.07 | 0.01 | 0.10 | 0.08 |
| 21 | 0.00 | 0.01 | 0.16 | 0.12 | 0.09 | 0.10 | 0.06 | 0.03 | 0.73 | 0.06 |
| 22 | 0.03 | 0.01 | 0.14 | 0.00 | 0.22 | 0.00 | 0.00 | 0.14 | 0.11 | 0.08 |
| 23 | 0.02 | 0.08 | 0.06 | 0.02 | 0.01 | 0.00 | 0.07 | 0.04 | 0.01 | 0.03 |

Figure 4 Matrix representation of the noise contaminated image

A traditional *K-means* clustering algorithm is applied to obtain the initial segmentation. The algorithm attempts to categorize the estimated site to the closest cluster center by the measurement in distance. Matrix in Figure 5 and its intensity image representation in Figure 7(b) are the initial segmentation by *K*-means indicating three higher level areas with region label 1 and other lower level area with region label 0. Three typical cells are highlighted to illustrate the Bayesian updating procedure. Cell D32 is a high grey value pixel with mainly high grey value neighbors; Cell F35 is a typical low grey value pixel with all lower grey value neighbors; and cell H29 is a typical high grey value pixel with lower grey value neighbors. When updating the segmentation label, the immediate neighboring information should be introduced by the formulation of GRF.

All the pixels in the image may be roughly classified into three categories mentioned above. The factor showing how they behave in the updating procedure is the different number of same label pixels in its neighboring system. For example, the 0.77 the cell D19 has 4 high level neighbors, while its right neighbor 0.8 only has two high level neighbors. Therefore 0.77 is more likely to belong to be cluster 1 than its neighbor 0.8.

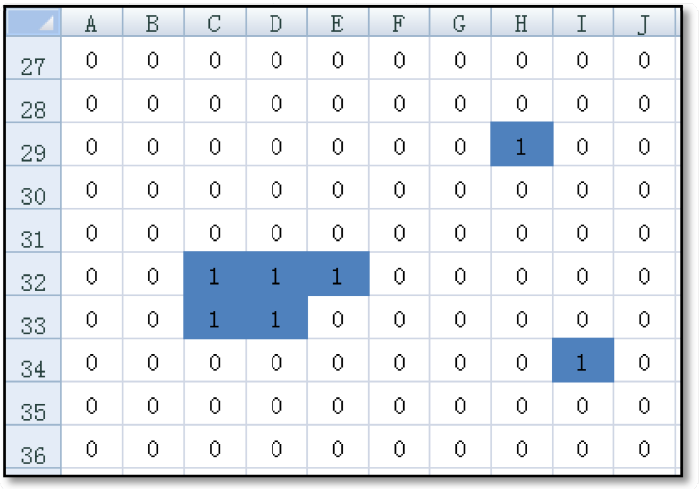

| | A | B | C | D | E | F | G | H | I | J |
|---|---|---|---|---|---|---|---|---|---|---|
| 27 | 0 | 0 | 0 | 0 | 0 | 0 | 0 | 0 | 0 | 0 |
| 28 | 0 | 0 | 0 | 0 | 0 | 0 | 0 | 0 | 0 | 0 |
| 29 | 0 | 0 | 0 | 0 | 0 | 0 | 0 | 1 | 0 | 0 |
| 30 | 0 | 0 | 0 | 0 | 0 | 0 | 0 | 0 | 0 | 0 |
| 31 | 0 | 0 | 0 | 0 | 0 | 0 | 0 | 0 | 0 | 0 |
| 32 | 0 | 0 | 1 | 1 | 1 | 0 | 0 | 0 | 0 | 0 |
| 33 | 0 | 0 | 1 | 1 | 0 | 0 | 0 | 0 | 0 | 0 |
| 34 | 0 | 0 | 0 | 0 | 0 | 0 | 0 | 0 | 1 | 0 |
| 35 | 0 | 0 | 0 | 0 | 0 | 0 | 0 | 0 | 0 | 0 |
| 36 | 0 | 0 | 0 | 0 | 0 | 0 | 0 | 0 | 0 | 0 |

Figure 5 Initial segmentation with traditional *K*-means clustering

To estimate the posterior probability, the mean value of each region needs to be calculated as follows:

For the class 0 (lower grey level cluster/ light area): $\mu^0 = 0.0692$

For the class 1 (higher grey level cluster/ dark area): $\mu^1 = 0.8440$

Pixels in all the images may be estimated with Eq. (5). Table1 lists three types of typical cells with index D19, H16, and F22 with the Gibbs potential parts given on the right side, indicating the adjustment procedure for each case.

The final segmentation result is given in Figure 7(c) which keeps the dominated high level zone and eliminates the isolated small ones. The results in matrix form are shown in Figure 6.

Table 1 Posterior calculation with Gibbs potential

| Cell Position | Posterior probability with Gibbs potential | Gibbs potential part |
|---|---|---|
| D19 | $p0 = \exp\left\{-\frac{1}{2\sigma^2}\left[y_s - \mu_s^0\right]^2 - \sum_C V_C(x=0)\right\}$ $= \exp\left\{-\frac{1}{2\sigma^2}[0.77 - 0.069]^2 - \sum_C V_C(x=0)\right\}$ | $\sum_C V_C = 0$ |
| | $p1 = \exp\left\{-\frac{1}{2\sigma^2}\left[y_s - \mu_s^1\right]^2 - \sum_C V_C(x=1)\right\}$ $= \exp\left\{-\frac{1}{2\sigma^2}[0.77 - 0.844]^2 - \sum_C V_C(x=1)\right\}$ | $\sum_C V_C = 0$ |

| | | |
|---|---|---|
| H16 | $p0 = \exp\left\{-\frac{1}{2\sigma^2}\left[y_s - \mu_s^1\right]^2 - \sum_C V_C(x=0)\right\}$ $= \exp\left\{-\frac{1}{2\sigma^2}[0.73-0.069]^2 - \sum_C V_C(x=0)\right\}$ | $\sum_C V_C = -8\beta$ |
| | $p1 = \exp\left\{-\frac{1}{2\sigma^2}\left[y_s - \mu_s^1\right]^2 - \sum_C V_C(x=1)\right\}$ $= \exp\left\{-\frac{1}{2\sigma^2}[0.73-0.844]^2 - \sum_C V_C(x=1)\right\}$ | $\sum_C V_C = 8\beta$ |
| F22 | $p0 = \exp\left\{-\frac{1}{2\sigma^2}\left[y_s - \mu_s^0\right]^2 - \sum_C V_C(x=0)\right\}$ $= \exp\left\{-\frac{1}{2\sigma^2}[0.00-0.069]^2 - \sum_C V_C(x=0)\right\}$ | $\sum_C V_C = -8\beta$ |
| | $p1 = \exp\left\{-\frac{1}{2\sigma^2}\left[y_s - \mu_s^1\right]^2 - \sum_C V_C(x=1)\right\}$ $= \exp\left\{-\frac{1}{2\sigma^2}[0.00-0.844]^2 - \sum_C V_C(x=1)\right\}$ | $\sum_C V_C = 8\beta$ |

| | A | B | C | D | E | F | G | H | I | J |
|---|---|---|---|---|---|---|---|---|---|---|
| 40 | 0 | 0 | 0 | 0 | 0 | 0 | 0 | 0 | 0 | 0 |
| 41 | 0 | 0 | 0 | 0 | 0 | 0 | 0 | 0 | 0 | 0 |
| 42 | 0 | 0 | 0 | 0 | 0 | 0 | 0 | 0 | 0 | 0 |
| 43 | 0 | 0 | 0 | 0 | 0 | 0 | 0 | 0 | 0 | 0 |
| 44 | 0 | 0 | 0 | 0 | 0 | 0 | 0 | 0 | 0 | 0 |
| 45 | 0 | 0 | 1 | 1 | 1 | 0 | 0 | 0 | 0 | 0 |
| 46 | 0 | 0 | 1 | 1 | 0 | 0 | 0 | 0 | 0 | 0 |
| 47 | 0 | 0 | 0 | 0 | 0 | 0 | 0 | 0 | 0 | 0 |
| 48 | 0 | 0 | 0 | 0 | 0 | 0 | 0 | 0 | 0 | 0 |
| 49 | 0 | 0 | 0 | 0 | 0 | 0 | 0 | 0 | 0 | 0 |

Figure 6 Bayesian segmentation with MRF prior

(a) (b) (c)

Figure 7 Comparison of (a) the original image and (b) *K*-means result and (c) Bayesian updated result

## 5. SEGMENTATION FOR F-K MIGRATION IMAGES

Imaging algorithms for diagnosing damage in plate-like structures have drawn continual interest. The time reversal scheme developed in time-space domain and frequency-wave number domain has been successfully verified its effectiveness and efficiency for damage detection. The migration imaging technique, based on Mindlin plate theory, is one of the most promising methods for multi-damage identification in plate-like structures using scattered Lamb waves in combination with the time-coincidence imaging condition.

The migration technique can effectively interpret the sensor data recorded by a distributed linear array sensor system and makes it possible to establish an active, in-service, and intelligent monitoring system. The image for segmentation is obtained from an active diagnostic linear array of actuators/sensors, which is used to excite/receive the flexural waves. The wave field scattered from the damage and sensor array data are synthesized using a two-dimensional explicit finite difference scheme to model wave propagation in the plate based on the Mindlin plate theory. The damage image can be represented by the cross-correlation in frequency domain as:

$$I(x,y) = \sum\nolimits_{\omega} w^{e*}(x,y,\omega) w^{s}(x,y,\omega) \tag{6}$$

in which $I(x,y)$ is the pixel value at $(x,y)$, $w^{e}(x,y,\omega)$ and $w^{s}(x,y,\omega)$ are the extrapolated excitation and scattered wave-fields in frequency domain, respectively.

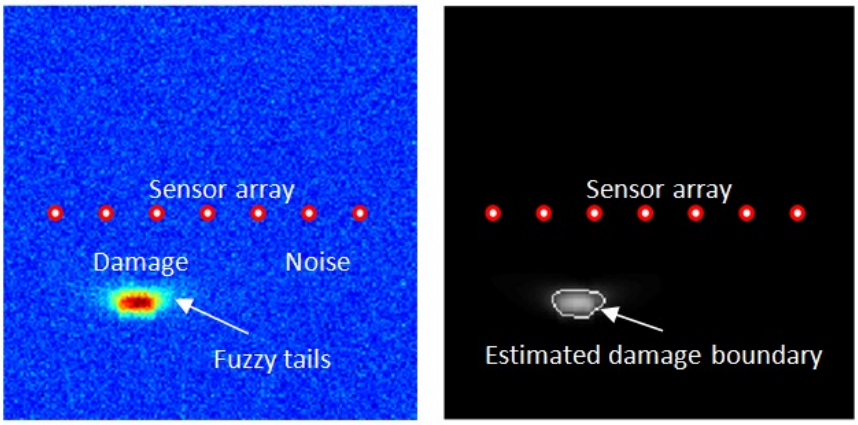


(a) (b)

Figure 8 (a) *f-k* migration image and (b) the Bayesian based segmentation

When *K*-means segmentation is applied to the *f-k* migration image, some of the medium grey-levels in the fuzzy tails will be segmented as the damaged area. Markov Random Field features the property of emphasizing the local constraint by

introducing the Gibbs potential in the posterior probability. Thus the damaged area from the segmentation shrinks regardless of ghost images. Figure 8(b) gives the segmentation result and its region resulting from Bayesian updating scheme. As a comparison, for a 20 mm crack case, the crack length obtained from the *K*-means (without noise) segmentation is 30 mm, while the estimated crack size obtained from Bayesian updating algorithm is 25 mm, providing more precise crack size estimation. Furthermore, the crack size estimated is larger than the true crack size, ensuring the conservative measure of the damage.

The parameter $\beta$ in the Gibbs potential plays an important role of the segmentation procedure. It determines how the neighboring system affects the label of the estimated site. When $\beta = 0$, the Bayesian segmentation reduces to the *K*-means clustering, which segments some of the noise area in the same region of the damaged area and the result is given in Figure 9(b). It is difficult to determine the crack length with such segmentation. With the increase in $\beta$, the noise is suppressed, and the damage area shrinks to the real damaged area. Results show that the segmentation does not change when $\beta$ varies from 0.9 to 100, which shows the stability of the segmentation. The reason for the convergence phenomenon is that the Gibbs potential provides plays only an adjustment role in the Bayesian updating procedure, but not a dominating role.

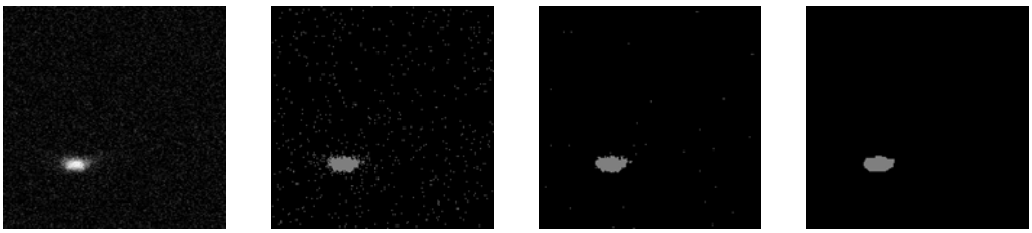

(a) Original (b) β=0 (c) β=0.1 (d) β=0.5

Figure 9 Bayesian based image segmentation with different Gibbs potentials

The resolution of the segmentation first depends on the quality of the image. For the imaging procedure using *f-k* migration technique, the center frequency of the excitation is 150 kHz as shown in Figure 10. The maximum frequency over 3% frequency magnitudes is about 244 *kHz*, and the thickness of the monitored aluminum plate in the simulation is 3.2 *mm*. The mainly excited mode in the simulation is the first-order asymmetric mode, $A_0$ mode. From the dispersive curve the velocity of $A_0$ mode for Lamb wave is 3.025 *m/ms*. Through Eq. (7), the wavelength for the highest frequency in the excitation signal can be obtained.

$$\lambda = \frac{v}{f} \tag{7}$$

The shortest wavelength in the excitation frequency band is 12.4 mm. Therefore, the estimated error of 5 mm in crack size is smaller than half of the shortest wavelength. To improve the accuracy of the crack size estimation, higher frequency excitation may be used. However there will be a tradeoff between the complexity of multi-modes in high frequencies and the image resolution.

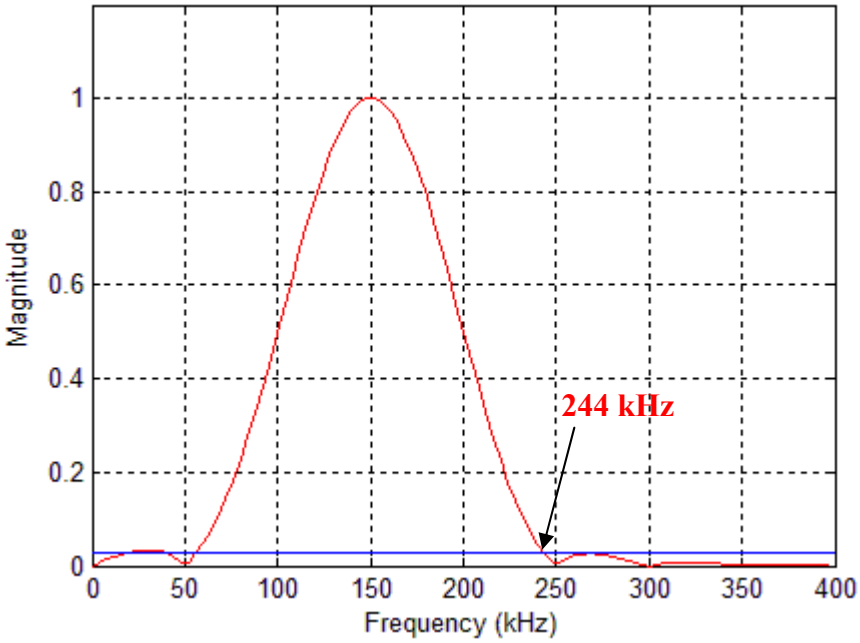


Figure 10 Excitation waveform in time-domain and frequency-domain

## 6. CONCLUSIONS

The proposed Bayesian based segmentation algorithm for estimating damage size has been shown to possess the following advantages: (1) Spatial constraint using the neighboring system is better than *K*-means clustering, which only considers the grey-level distance between the pixels and the clustering centers. As a result, the damage area is focused suppressing the fuzzy tails that may appear on both crack tips. (2) Bayesian based segmentation holds the promise of reducing noise by applying the Gibbs Random field, which assumes that neighboring pixels more likely belong to be the same class. (3) The segmentation result gives damage shape and region estimation of the damaged area. In other words, the Bayesian updating with the MRF as a prior can efficiently segment an image into multiple regions, which distinguishes damaged regions from undamaged regions. For future work, the segmentation results can also be used as prior information for the next Bayesian updating scheme, thereby enhancing the current image. Furthermore, different diagnostic techniques that form the images can contribute to Bayesian updating and makes the segmentation more precise and reliable.

## 7. ACKNOWLEDGEMENT

The authors gratefully acknowledge the support of the research by the U.S. Air Force under Grant FA9550-07-1-0018 and by the NASA under Grant NNX08AC334.

## REFERENCES

1. L. Wang and F. G. Yuan, "Active Damage Localization Technique based on Energy Propagation of Lamb Waves," *Smart Structures and Systems*, 3(2), 201-217(2007).
2. V. Giurgiutiu, L. Yu, K. James and R. J. Christopher, "In Situ Imaging of Crack Growth with Piezoelectric-Wafer Active Sensors," *AIAA Journal*, 45(11), 2758-2769(2007).
3. Y. Gómez-Ullate and F. Montero de Espinosa, "Non Destructive Evaluation of Carbon Fiber Reinforced Plates Using Lamb Waves: A Comparison between Pitch-Catch Air Coupled Techniques and Sector Images Obtained with Embedded Piezoelectric Linear Arrays," *Ultrasonics Symposium, IEEE*, 593-596(2007).

4. L. Wang and F. G. Yuan, "Damage identification in a composite plate using prestack reverse-time migration technique," *Structural Health Monitoring*, 4(3), 195-211(2005).
5. X. Lin and F. G. Yuan, "Damage Detection of a Plate Using Migration Technique," *Journal of Intelligent Material Systems and Structures*, 12(7), 469-482(2001).
6. X. Lin and F. G. Yuan, "Detection of Multiple Damages by Prestack Reverse-time Migration," *AIAA* 39(11), 2206-2215(2001).
7. X. Lin and F. G. Yuan, "Experimental Study Applying a Migration Technique in Structural Health Monitoring," *Structural Health Monitoring*, 4(4), 341-353(2005).
8. P. C. Paris, M. P. Gomez and W. E. Anderson, "A Rational Analytic Theory of Fatigue," *The Trend in Engineering*, 13, 9-14(1961).
9. A. Ishimaru, "Acoustical and Optical Scattering and Imaging of Tissues--An Overview," *Medical Imaging 2001: Ultrasonic imaging and signal processing*, *Proceedings of SPIE*, 4325, 1-10(2001).
10. J. A. Noble and D. Boukerroui, "Ultrasound Image Segmentation: A Survey," *IEEE Transactions on Medical Imaging*, 25(8), 987-1010(2006).
11. S. Geman and D. Geman, "Stochastic Relaxation, Gibbs Distributions, and the Bayesian Restoration of Images," *IEEE Transactions on Pattern Analysis and Machine Intelligence*, 6(6), 721-741(1984).
12. T. N. Pappas, "An Adaptive Clustering Algorithm for Image Segmentation," *IEEE Transactions on Signal Processin*g, 40(4), 901-914(1992).
13. J. Besag, "On the Statistical Analysis of Dirty Pictures," *Royal Statistics Society*, 48(3), 259-302(1986).
14. J. B. MacQueen, "Some Methods for Classification and Analysis of Multivariate Observations," *Proceedings of 5-th Berkeley Symposium on Mathematical Statistics and Probability*, Berkeley, University of California Press, 281-297(1967).
15. T. Bayes, "An Essay towards Solving a Problem in the Doctrine of Chances. By the late Rev. Mr. Bayes, F. R. S. communicated by Mr. Price, in a letter to John Canton, A. M. F. R. S.," *Philosophical Transactions*, 53, 370-418(1763).
16. X. Lin and F. G. Yuan, "Experimental Study Applying a Migration Technique in Structural Health Monitoring," *Structural Health Monitoring*, 4(4), 341-353(2005).
17. J. B. Ihn and F. K. Chang, "Pitch-Catch Active Sensing Methods in Structural Health Monitoring for Aircraft Structures," *Structural Health Monitoring*, 7(1), 5-19 (2008).
18. R. Kindermann and J. L. Snell, *Markov Random Field and Their Applications*, American Mathematical Society, 1980. http://www.ams.org/online_bks/conm1/
19. S. Z. Li, *Markov Random Field Models in Computer Vision*, Springer-Verlag Berlin Heidelberg, 1994.
20. M. DeGroot, *Optimal Statistical Decisions*, McGraw-Hill, 1970.